

**Data Mining Inspired Localized Resistivity in Global
MHD Simulations of the Magnetosphere**

H. Arnold¹, K. Sorathia¹, G. Stephens¹, M. Sitnov¹, V.G. Merkin¹, J. Birn²

¹Johns Hopkins Applied Physics Laboratory, Laurel, MD USA

²Space Science Institute, Boulder, CO USA

Key Points:

- Localized Resistivity in global MHD simulations can “encourage” magnetic reconnection in specific locations to match data mining results
- Active x-lines at $X_{GSM} \lesssim -20R_E$ can suppress the formation of extended x-lines at $X_{GSM} \gtrsim -15R_E$
- Reconnection outflows rebound from the near-Earth region causing transient and narrow (in Y_{GSM}) secondary reconnection

13 **Abstract**

14 Recent advances in reconstructing Earth's magnetic field and associated currents by uti-
 15 lizing data mining of in situ magnetometer observations in the magnetosphere based on
 16 geomagnetic indices and solar wind parameters have proven remarkably accurate at re-
 17 producing observed ion diffusion regions. We investigate the effect of placing regions of
 18 localized resistivity in global simulations of the magnetosphere at specific locations in-
 19 spired by the data mining results for the substorm occurring on July 6, 2017. When ex-
 20 plicit resistivity is included, the simulation forms an x-line at the same time and loca-
 21 tion as the MMS observation of an ion diffusion region at 15:35 UT on that day. With-
 22 out this explicit resistivity, reconnection forms later in the substorm and far too close
 23 to Earth ($\gtrsim -15R_E$), a common problem with global simulations of Earth's magneto-
 24 sphere. A consequence of reconnection taking place farther down the tail due to local-
 25 ized resistivity is that the reconnection outflows transport magnetic flux Earthward and
 26 thus prevent the current sheet from thinning enough for reconnection to take place nearer
 27 Earth. As these flows rebound tailward from the inner magnetosphere, they can tem-
 28 porarily and locally (in the dawn-dusk direction) stretch the magnetic field allowing for
 29 small scale x-lines to form in the near Earth region. Due to the narrow cross-tail extent
 30 of these x-lines ($\lesssim 5R_E$) and their short lifespan ($\lesssim 5\text{min}$), they would be difficult to
 31 observe with in situ measurements. Future work will explore time-dependent resistiv-
 32 ity using 5 minute cadence data mining reconstructions.

33 **Plain Language Summary**

34 Recently, data mining of spacecraft magnetometers have created highly accurate
 35 reconstructions of Earth's magnetic field. These reconstructions capture the location and
 36 timing of so called x-lines on the night side of Earth. Magnetic field lines reconnect at
 37 x-lines and convert magnetic energy to plasma energy via heating and acceleration of
 38 flows. Nightside reconnection is a crucial part of geomagnetic storms and substorms that
 39 pose a danger to spacecraft, astronauts, and the power grid on Earth. By identifying x-
 40 lines in reconstructions we can influence simulations of specific substorms to increase their
 41 accuracy and make them more physically realistic. We demonstrate this ability by match-
 42 ing simulation results with observations and find that reconnection further from Earth
 43 suppresses extended x-line formation near Earth. Additionally, the flows from reconne-
 44 ction can bounce off the strong magnetic field close to Earth (a well known effect) and
 45 locally stretch the magnetic field creating small scale x-lines near Earth.

46 **1 Introduction**

47 Earth's magnetosphere is a dynamic system driven by the solar wind. Magnetic
 48 reconnection on the day side transfers magnetic flux to the night side, gradually increasing
 49 the magnetic energy density in the tail lobes during the growth phase of a substorm.
 50 At some point the expansion phase is explosively triggered, likely due to demagnetiza-
 51 tion of ions (Schindler, 1974; Sitnov & Schindler, 2010; Sitnov et al., 2013; Bessho & Bhat-
 52 tacharjee, 2014; Pritchett, 2015) or electrons (Coppi et al., 1966; Hesse & Schindler, 2001;
 53 Liu et al., 2014), and the stored energy in the lobes is released through magnetic recon-
 54 nection (Baker & P, 1996; Angelopoulos et al., 2008). This results in the dipolarization
 55 of the nightside magnetic field (Russell & McPherron, 1973).

56 Modelers have successfully simulated many of the observed features of substorms,
 57 including magnetotail reconnection and resulting dipolarization (e.g. Birn et al., 1996;
 58 Raeder, 2003; Merkin et al., 2019). However, no single simulation can correctly simu-
 59 late all the physics due to the several orders of magnitude difference between kinetic and
 60 global scales. This has led to different efforts to understand the relevant physics, but there
 61 are still many questions unanswered. Notably, where and when does magnetic reconne-
 62 ction take place in the magnetotail and how does that affect the global system?

We investigate this question in the context of a global magnetohydrodynamic (MHD) simulation, but also consider the important role non-MHD effects play in determining the location and timing of reconnection in the magnetotail. Prior to reconnection onset, the tail current sheet may have a multiscale structure with an ion-scale thin current sheet embedded in a thicker plasma sheet (Sergeev et al., 2011) or it may be bifurcated on similar ion scales (Nakamura et al., 2002; Runov et al., 2003, 2005, 2006; Sergeev et al., 2003). While Birn and Schindler (2002) have demonstrated that thin current sheets can form even within a quasi-static isentropic model with isotropic pressure (equivalent to slow ideal MHD evolution), other approaches have indicated the possibly important role of pressure anisotropy (Artemyev et al., 2021). Further, during, or even prior to, reconnection the current sheet thins even more down to electron scales (Torbert et al., 2018). Additionally, several studies indicate that x-lines are commonly expected and observed to be near $-40R_E < X_{GSM} < -20R_E$ (L. Q. Zhang et al., 2010; Nagai et al., 1998; Imber et al., 2011; Zhao et al., 2016) in the Geocentric Solar Magnetosphere (GSM) coordinate system. However, extended x-lines are often seen too close to the Earth in global MHD simulations (El-Alaoui et al., 2009; Gong et al., 2021; Bard & Dorelli, 2021; Park, 2021) (see also Fig. 3 (a)) and even in Hall MHD or hybrid simulations (Bard & Dorelli, 2021; Runov et al., 2021).

Recently, data mining (DM) has been harnessed to reconstruct the state of the magnetosphere for a given point in time (G. Stephens et al., 2019; G. K. Stephens et al., 2022). In order to test the accuracy of this method the authors examined $B_{z,GSM} = 0$ contours in the magnetotail current sheet and compared them to Magnetospheric Multiscale Mission (MMS) observations of ion diffusion regions (IDRs). Ions decouple from the magnetic field in IDRs where the Earth-Sun magnetic field and the north-south magnetic field reverse and thus IDRs are useful for identifying features in the magnetic field geometry such as x- and o-lines (Rogers et al., 2019). The authors were able to show these contours were within $1R_E$ of an MMS identified IDR for 16 out of 26 total IDRs. 8 others were within $1R_E$ of a $2nT$ contour, signifying that DM was close to resolving the reconnection site (G. K. Stephens et al., 2022). This is especially impressive since one of the misses occurred during a time of weak magnetospheric activity and the other was during a gap in solar wind data. While (G. K. Stephens et al., 2022) has not yet been published, they have provided a detailed uncertainty evaluation that makes their comparison with MMS data extremely convincing. By identifying the location of x-lines in the reconstruction and placing localized resistivity in these regions in the MHD simulation, we can effectively take non-MHD physics into account and “encourage” the simulation to form an x-line where and when we expect there to be reconnection from the DM results. Without this intervention the crucial process of tail reconnection will not occur at the correct time or location, which will affect the global response of the magnetosphere.

This paper presents results from different simulations that all model the substorm that took place on July 6, 2017 from approximately 15:35 to 17:00. We demonstrate that a localized resistivity can successfully induce reconnection in different locations in the tail. An unexpected result is that reconnection farther down the tail may actually suppress near-Earth reconnection by transporting magnetic flux there and preventing the current sheet from collapsing. However, due to the 3D nature of the tail, the magnetic field can be stretched again by rebounding flows resulting in smaller, transient x-lines in the near-Earth region. These rebounding flows are a well known feature observationally (e.g. Ohtani et al., 2009) and have been found in global simulations as well (e.g. Merkin et al., 2019). However, the additional reconnection they can create has not yet been discussed.

In section 2 we describe the simulations that we examine and the methodology for identifying x-lines in our simulations. In section 3 we show that DM inspired localized resistivity can create x-lines that match observations. In section 4 we explain how re-

connection farther in the tail suppresses extended x-line near Earth. In section 5 we present evidence of small x-lines that form in rebounding flows. And in section 6 we conclude.

2 Event Description and Simulation Setup

We perform simulations using the global magnetohydrodynamic code GAMERA (B. Zhang et al., 2019; Sorathia et al., 2020) coupled with the ionospheric potential solver REMIX (Merkin & Lyon, 2010), which used a constant conductance of $5S$. Our simulations consist of a distorted spherical grid and a cylinder as the boundary with the faces located at $X_{SM} = 30R_E$ and $X_{SM} = -330R_E$ in the Solar Magnetic (SM) coordinate system. Note that both GSM and SM have the same Y-axis, but Z_{GSM} points along Earth's north magnetic pole and X_{SM} points directly toward the sun. The radius of the cylinder is $110R_E$ and it consists of $96 \times 96 \times 128$ grid cells in the radial, polar, and azimuthal dimensions respectively. This leads to a grid cell of length $\sim 0.5R_E$ at $X_{GSM} = -20R_E$. The magnetosphere is driven using data from the OMNI database for the period on July 6, 2017 from 14:35-17:35. The Sym-H magnitude remained small for the entirety of the simulation indicating that the ring current is not important to magnetospheric dynamics. Prior to the simulation, there is a spin-up period of two hours where a dipole magnetosphere is driven by a hydrodynamic solar wind corresponding to the initial values on the left side of Fig. 1. All of our simulations result in substorm dynamics due to the southward turning IMF magnetic field.

In this paper we examine 3 simulations: one with only numerical resistivity to break the frozen in theorem and allow reconnection (Run Base), one with localized resistivity placed near $X_{GSM} \sim -30R_E$ (Run Mid) and one with localized resistivity placed at a location inspired from DM reconstructions (Run DM_Reconst). The location is specified by X_{SM} , Y_{SM} , and Z_{SM} coordinates with varying widths in each direction. The resistivity in our simulations is defined as

$$\eta = \eta_0 / \cosh^2 \left[\left(\frac{x - x_0}{L_x} \right)^2 + \left(\frac{y - y_0}{L_y} \right)^2 + \left(\frac{z - z_0}{L_z} \right)^2 \right] \quad (1)$$

where x_0 , y_0 , and z_0 give the center of the resistive region in SM coordinates, $\eta_0 = 40,000\Omega m$ as in (Hesse & Birn, 1994), $L_x, L_y, L_z = 2.5, 10, 12.5R_E$ for Run Mid, and $L_x, L_y, L_z = 3, 5, 2R_E$ for Run DM_Reconst. L_x is chosen to be small enough to isolate the location of the resulting x-line in the tail, but must be larger than the DM resolution of $1R_E$ and the inherent variation of the DM x-line. L_y is similarly chosen to capture the full x-line as seen in the DM reconstruction, but also chosen so as not to include the magnetopause. Finally, L_z is chosen to include the current sheet and avoid the magnetopause. Further reduction of L_z may be risky because DM cannot reproduce mesoscale motions of the tail current sheet associated with flapping and buoyancy motions (e.g. Runov et al., 2005; ?, ?). So L_z should be sufficiently large to mitigate these effects. Although these values are somewhat ad hoc they have already provided insight into reconnection in the magnetotail. In future papers these values will be refined to closely match the DM reconstructions. Calculating the relevant scales from Run Mid in the resistive region, we find a length of $\sim 1R_E$ for the width of the current sheet in the Z_{GSM} direction, and a characteristic upstream Alfvén speed of $\sim 1000\text{km/s}$ which gives a Lundquist number of $S = LU\mu_0/\eta \sim 200$ where μ_0 is vacuum permeability. Additionally, η_0 must be chosen to be large enough to have a noticeable effect on the simulation, but small enough so as not to increase the resulting time step too much. A large resistivity results in a large diffusive velocity that must be resolved by the time step. We decreased the value of resistivity in a separate simulation (not shown) by an order of magnitude, and in that case the localized region of resistivity was unable to lead to substantial reconnection. While more experimenting could have reduced η_0 further, we decided to keep the value the same as in previous papers since it is sufficient to cause reconnection but not large enough to substantially increase the simulation cost.

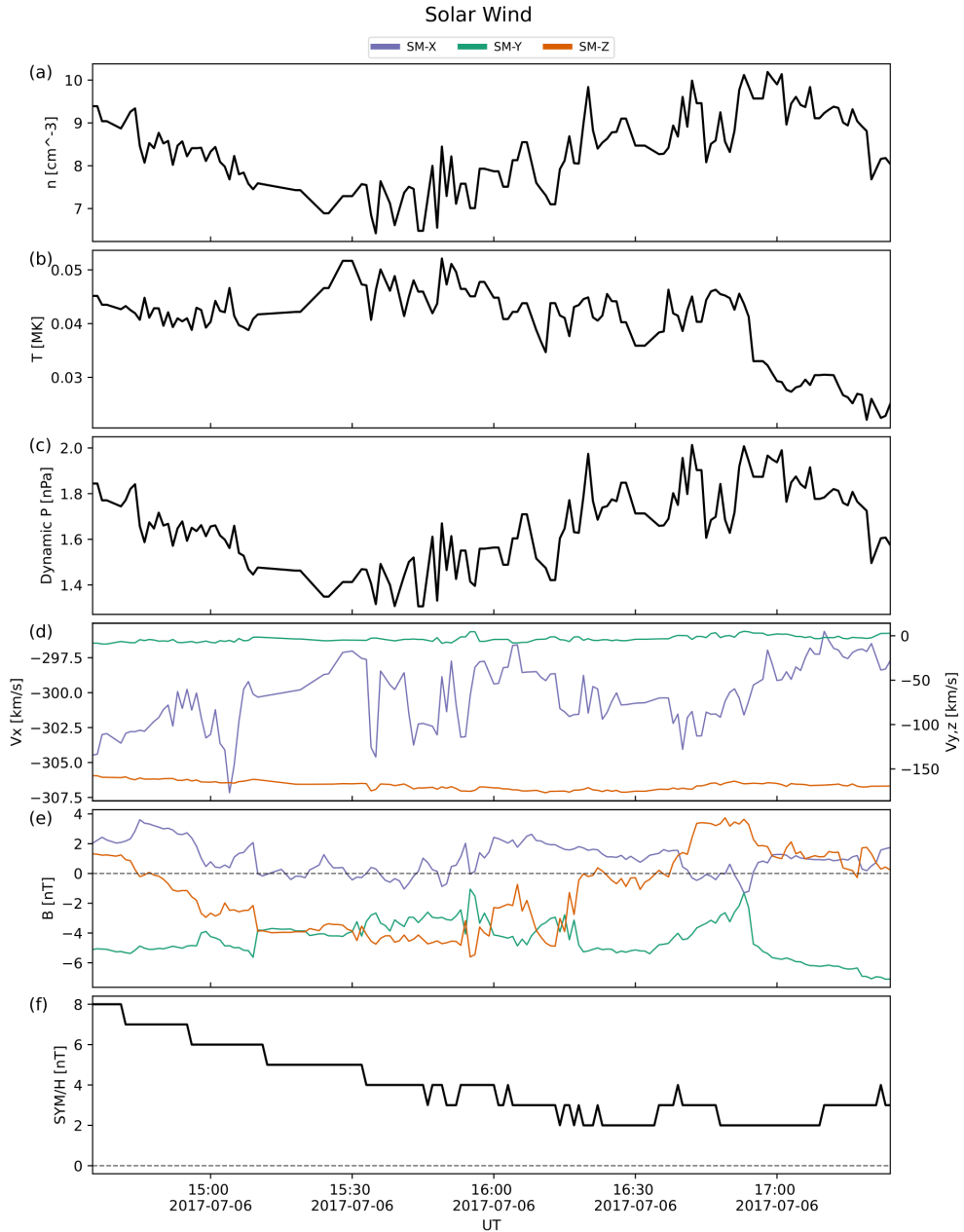


Figure 1. Solar wind parameters from the National Aeronautics and Space Administration OMNI database for the period of our simulations. (a) density, (b) temperature, (c) dynamic pressure, (d) flow velocity, (e) magnetic field, and (f) SYM-H index. The vector quantities are in Solar Magnetic Coordinates.

158 In order to explore the effects of resistivity, we developed a method to identify the
 159 location of x-lines. Since we are primarily interested in tail reconnection, we limited our-
 160 selves to the region $-60 < X_{GSM}/R_E < -5$, $-10 < Y_{GSM}/R_E < 10$, and $-10 < Z_{GSM}/R_E < 10$. Further, we required that the azimuthal current (in GSM coordinates)
 161 be larger than $\sim 0.5 A/m^2$ and that both $B_{Z,GSM}$ and $B_{X,GSM}$ reverse sign within 1
 162 grid cell of the suspected x-line location. Then we trace the magnetic field lines for $3R_E$
 163 in the $X_{GSM}-Z_{GSM}$ plane, both parallel and anti-parallel to \mathbf{B} , starting at $X_{GSM} \pm$
 164 $1R_E$ from the identified cell. The result is 4 different locations where, assuming the iden-
 165 tified cell is an x-line, both ends of the field line that started on the Earthward side of
 166 the cell in question will remain on the Earthward side and, similarly, field lines that start
 167 on the tailward side will remain on the tailward side. However, we only require 3 of the
 168 final locations to follow this pattern as the reconnecting magnetic field is not guaran-
 169 teed to perfectly lie along X_{GSM} . The resulting identified x-lines have been verified to
 170 have a general agreement with the expected geometry. However, they tend to be spread
 171 out in the X_{GSM} and Y_{GSM} directions in the vicinity of an x-line which introduces some
 172 unavoidable error.
 173

174 3 Localized Resistivity Induces Reconnection

175 There have been many studies of the magnetotail with resistive MHD simulations,
 176 and in particular MHD simulations with localized patches of resistivity (Hesse & Birn,
 177 1994; Raeder et al., 1996; Raeder, 1999; Raeder et al., 2001; Birn & Hesse, 2013). These
 178 have shown that a localized region of resistivity can induce reconnection locally (Ugai
 179 & Tsuda, 1979; Min et al., 1985; Scholer & Otto, 1991). However, until now there has
 180 been no way to reliably inform the simulation about where and when reconnection should
 181 take place in the magnetotail. Using the magnetosphere reconstruction results from DM,
 182 we can determine the location of reconnection with reasonable accuracy. And by strate-
 183 gically placing localized resistivity we will be able to induce reconnection that approx-
 184 imately matches both the spatial and temporal profiles of real, extended x-lines in a given
 185 substorm according to DM reconstructions.

186 As a first step we looked at the x-line that was identified by the MMS on July 6,
 187 2017 at $[X_{GSM}, Y_{GSM}, Z_{GSM}] = [-24.1, 1.41, 4.44]R_E$ (Rogers et al., 2019). In order
 188 to match the location of the observed x-line, we placed a region of resistivity as described
 189 above to induce reconnection in the appropriate place as determined from the DM re-
 190 construction of the magnetosphere (G. Stephens et al., 2019; G. K. Stephens et al., 2022).
 191 The comparison with the simulation without resistivity as well as the DM results can
 192 be seen in Fig. 2. Panel (a) shows the DM results in the $X'_{GSM} - Z_{GSM}$ plane where
 193 X'_{GSM} includes a small component of Y_{GSM} as seen by the dashed line in panel (b), (b)
 194 is the DM results in the $X_{GSM} - Y_{GSM}$ plane, (c) is at the same time but from Run
 195 Base in the $X_{GSM} - Z_{GSM}$ plane, (d) is in the $X_{GSM} - Y_{GSM}$ plane, and (e)-(f) are
 196 the same as (c)-(d) but from Run DM_Reconst. The result is a significant difference in
 197 the development of the magnetosphere. While both simulations form a geometric x-line
 198 deep in the tail near $X_{GSM} \sim -40R_E$ on the dawn side, it is not an active site of re-
 199 connection as can be seen by the lack of flow vectors in Fig. 2. Only the simulation with
 200 a localized resistivity leads to reconnection geometry with outflows near $\sim -25R_E$ in
 201 excellent agreement with in situ observations.

202 4 Mid-Tail Reconnection Suppresses Near Earth Reconnection

203 The above demonstrates that we can induce reconnection with localized resistiv-
 204 ity and that we can match observations of ion diffusion regions with x-lines in a simu-
 205 lation at the correct place and time. However, to consider a more generalized case, we
 206 also look at a simulation with resistivity located in the region $X_{GSM} \sim -30R_E$, Run
 207 Mid. This is because of observations suggesting this as the likely location of near Earth

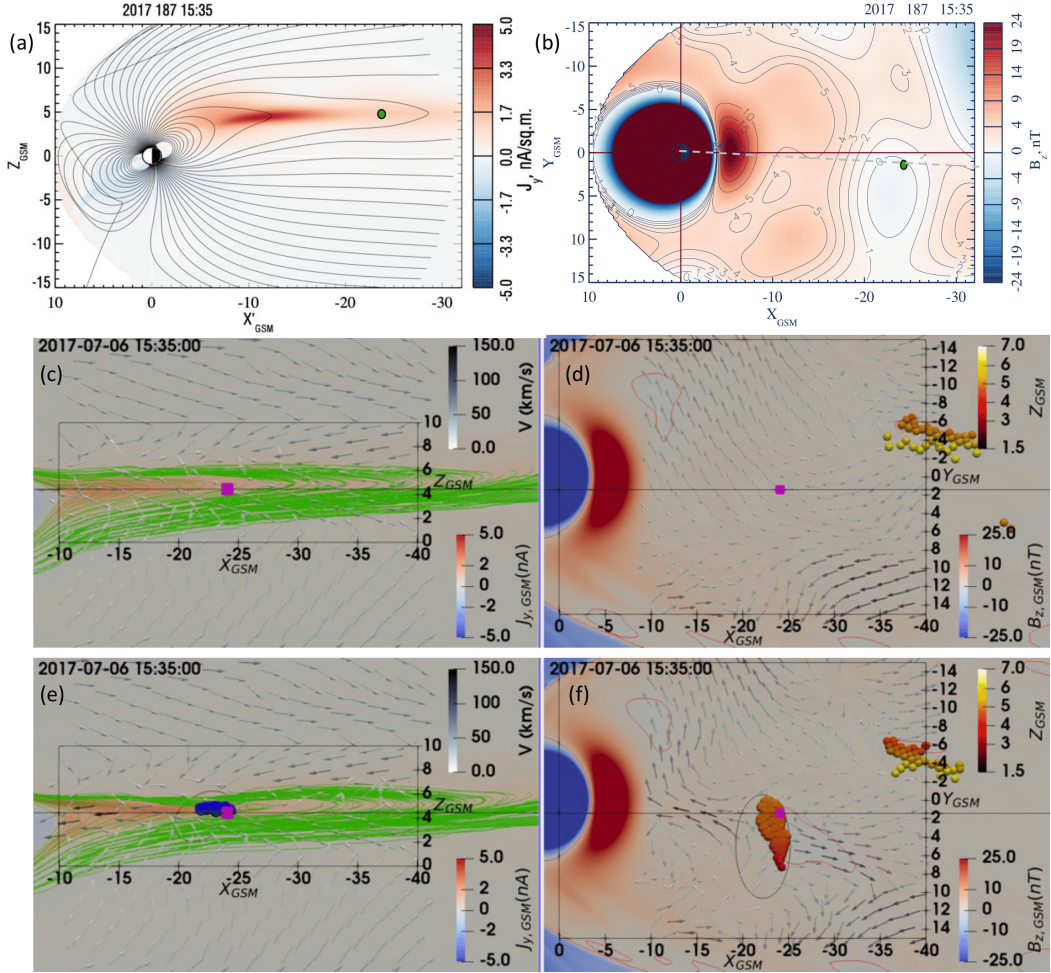


Figure 2. Each figure corresponds to July 6, 2017 at 15:35. Panel (a) and (b) show the DM reconstruction of the magnetosphere in the $X'_GSM - Z_GSM$ and $X_GSM - Y_GSM$ ($Z_GSM = 4.2R_E$) planes respectively. (a) is the current in the Y_GSM direction with field lines in black. (b) is $B_{Z,GSM}$ with contours equal to $B_{Z,GSM} = 0, 2, 3$ and $4nT$. The location of MMS is depicted by a green circle in both panels where it observed an ion diffusion region. The dashed line in (b) shows the location of the plane of (a) and the X'_GSM axis. Panels (c) and (d) are the $X_GSM - Z_GSM$ and $X_GSM - Y_GSM$ plane respectively from Run Base. (c) shows $J_{Y,GSM}$ with selected field lines in green, and (d) shows $B_{Z,GSM}$ with contours of $B_{Z,GSM} = 0$ in red. Both panels show flow vectors as white arrows. The horizontal lines in each plane corresponds to the location of the plane in the other panel. The pink squares are the location of MMS. The circles are the location of identified x-lines in the simulation, in (d) and (f) they are colored according to their Z_GSM location. (c) and (e) only show identified x-lines within $1R_E$ of the plane. Panels (e) and (f) are the same as (c) and (d) respectively except for Run DM_Reconst. The black circles correspond to contours of resistivity equal to $10,000\Omega m$.

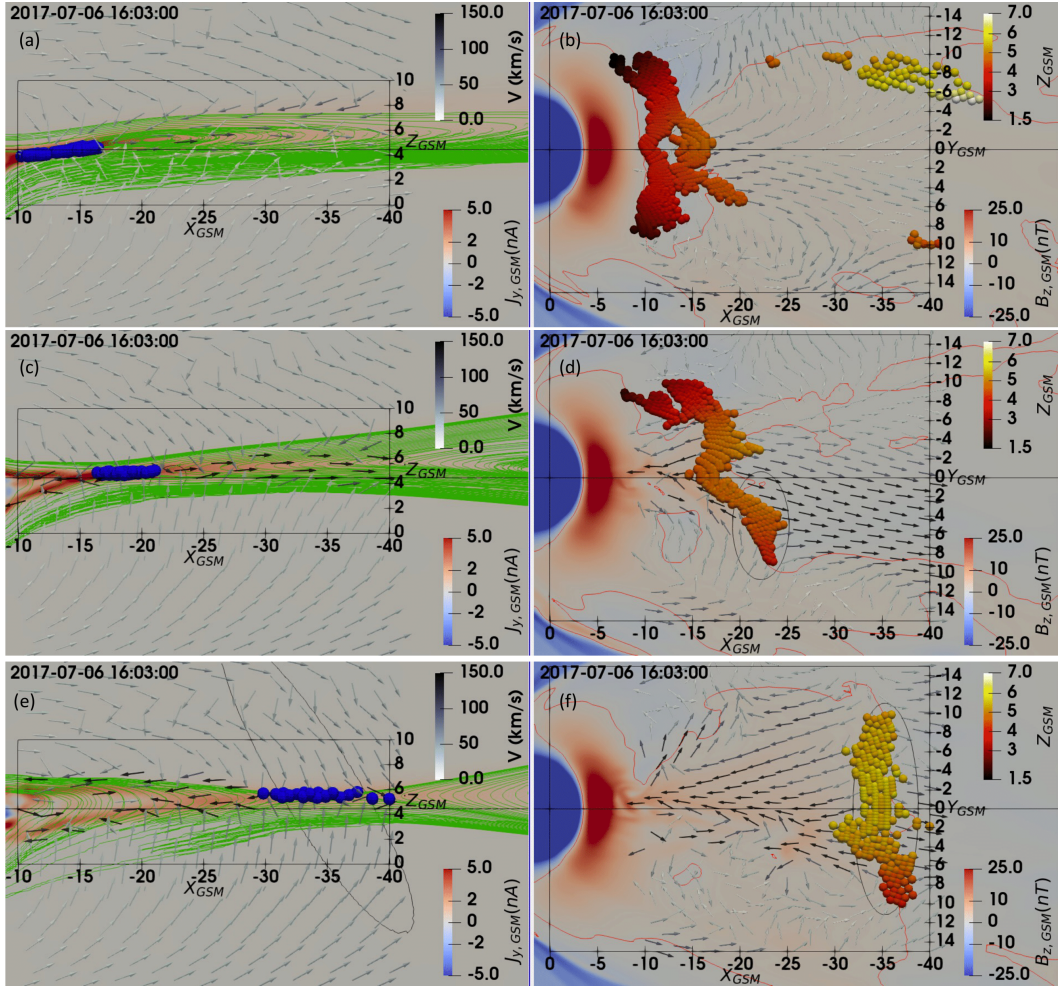


Figure 3. Each pair of panels in this figure have the same format as Fig. 2 (c)-(d). However, they are at a time shortly after reconnection begins in Run Base and they lack the location of MMS. (a) and (b) are from Run Base, (c) and (d) are from Run DM_Reconst and (e) and (f) are from Run Mid.

reconnection (Imber et al., 2011; Zhao et al., 2016) as well as the consistent and extended x-lines that the DM results suggest exist here (G. K. Stephens et al., 2022), thus Run Mid is also inspired by DM results. A snapshot of Run Base compared with Run DM_Reconst and Run Mid can be seen in Fig. 3. An important consequence is that the resistivity induced reconnection in both Run DM_Reconst and Run Mid creates diverging flows sooner. The Earthward flow transports flux to the near Earth region which prevents the current sheet from narrowing and thus suppresses near Earth reconnection that would otherwise take place. This is especially evident in Run Mid, but even in Run DM_Reconst the x-lines are generally deeper in the tail. This process is what dipolarizes the inner magnetosphere and naturally prevents reconnection there.

Without explicit resistivity any reconnection in this region (near $X_{GSM} \lesssim -30R_E$) is unsteady and is not extended along the dawn-dusk region. Fig. 4 illustrates this point quite clearly. To form this figure we group all identified x-lines within $2R_E$ of each other, take the average X_{GSM} location, calculate the extent in the dawn-dusk direction as the width, and the center in the dawn-dusk direction as the Y_{GSM} location. Thus each “x”

223 is colored according to its Y_{GSM} location, plotted according to the time it occurred and
 224 its X_{GSM} location, and the size illustrates its width. We show the results for all three
 225 simulations. Finally, the observed AL index is also plotted for reference. Interestingly,
 226 all simulations form x-lines in the midtail region (near $X_{GSM} \sim -30R_E$) before the sub-
 227 storm onset. However, in Run Base and Run DM_Reconst the x-lines are smaller in width,
 228 tend to drift tailward, and seemingly jump around in X_{GSM} . Crucially, these x-lines are
 229 geometric only and remain inactive since they do not create diverging flows that are char-
 230 acteristic of reconnection. Shortly after the growth phase begins, an extended x-line forms
 231 in the near Earth region for Run Base, initially on the dusk side, and gradually retreats
 232 in the expansion phase.

233 For Run DM_Reconst the resistivity induces reconnection on the dusk side near $X_{GSM} \sim$
 234 $-20R_E$ just before the start of the growth phase. As the substorm progresses, the x-line
 235 gradually extends farther and farther towards the dawn until it occupies most of the tail
 236 as can be seen in Fig. 3 (d). This stretching of the x-line is also why the x-line appears
 237 to approach Earth. In fact, the x-line on the dusk side stays within the region of resis-
 238 tivity at $X_{GSM} \sim -20R_E$, but approaches Earth on the dawn side. Note that even though
 239 the average X_{GSM} position approaches Earth, it still generally stays farther in the tail
 240 than in Run Base, especially near the midnight line and duskward as can be seen in Fig.
 241 3. However, on the dawn side reconnection is not suppressed in the near Earth region
 242 since the magnetic flux from further in the tail has not been transported to this loca-
 243 tion as can be seen by the flow vectors in Fig. 3 (d). The x-line then retreats and even-
 244 tually breaks up in the recovery phase.

245 By placing resistivity farther in the tail we initially see a similar result. The x-line
 246 forms, but then extends in the dawn-dusk direction, and stays roughly constant well into
 247 the expansion phase. While this x-line stays roughly centered on the midnight line, it
 248 extends well into both the dawn and dusk sides. It is likely that the x-line is matching
 249 the region of resistivity as expected. Near the recovery phase the x-line finally begins
 250 to breakup before effectively disappearing altogether.

251 5 Rebounding Flows Stretch the Tail and Create Secondary X-Lines

252 The previous section clearly described how reconnection farther in the tail suppresses
 253 reconnection closer to Earth. However, as can be seen in Fig. 4 (c) there are some near
 254 Earth x-lines. These x-lines differ qualitatively from the near Earth x-lines in Run Base.
 255 Crucially, these x-lines do not last as long nor do they spread as far in the dawn-dusk
 256 direction. Additionally, they tend to form in rebounding flows. Rebounding flows are Earth-
 257 ward flows from reconnection that rebound tailward due to the strong magnetic field near
 258 Earth (Ohtani et al., 2009).

259 As an example of one of these x-lines in Run Mid consider Fig. 5. Panels (a) and
 260 (b) are similar to Fig. 3 (c) and (d) but zoomed in and at a different time. This is taken
 261 right after the x-line forms and clearly demonstrates that it forms in the tailward flow
 262 region as the reconnection outflow rebounds near Earth. Panels (c)-(f) depict various
 263 quantities as measured at one of the actual positions that the x-line forms, $[x, y, z] =$
 264 $[-11.05, 0.5, 4.31]$. However, since the x-line is tilted with respect to the x-axis as can
 265 be seen in panel (a), we define $B_{x,r}$ and $B_{z,r}$ to be the reconnecting and reconnected com-
 266 ponent of the magnetic field respectively. The vertical red dashed line indicates when
 267 the flow switches from Earthward to tailward and the vertical green line indicates when
 268 reconnection is observed. Shortly after the flow turns tailward the field lines continue
 269 to stretch as can be seen in the reduction of $B_{z,r}$ leading to secondary reconnection. These
 270 secondary x-lines were also observed in Run DM_Reconst as can be seen by the small
 271 red “x”s in Fig. 4 (b). This suggests that this secondary reconnection may be a com-
 272 mon consequence of midtail reconnection.

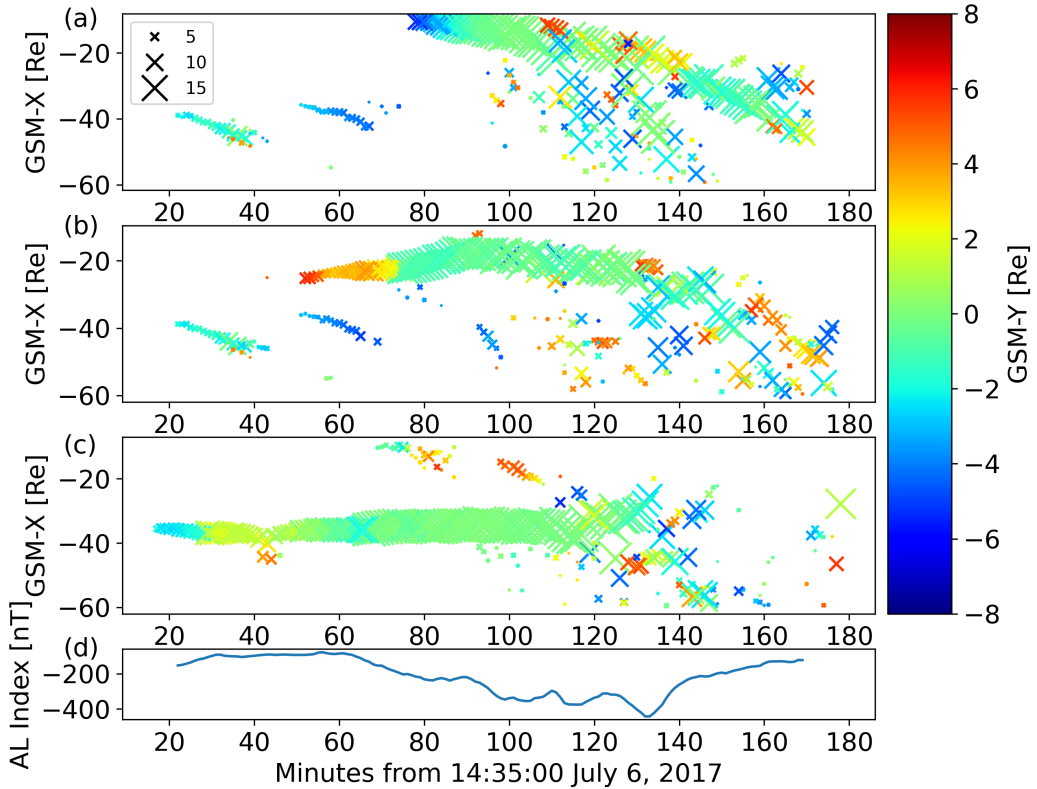


Figure 4. Panel (a) shows the x-lines seen throughout Run Base. Each “x” represents all identified x-lines within $2R_E$ of each other. The legend relates the size of each “x” to the width in the dawn-dusk direction in R_E . The color indicates the center of the x-line in the dawn-dusk direction. Panels (b) and (c) are the same as (a) but for Run DM_Reconst and Run Mid respectively. Panel (d) is the observed AL index during this time period.

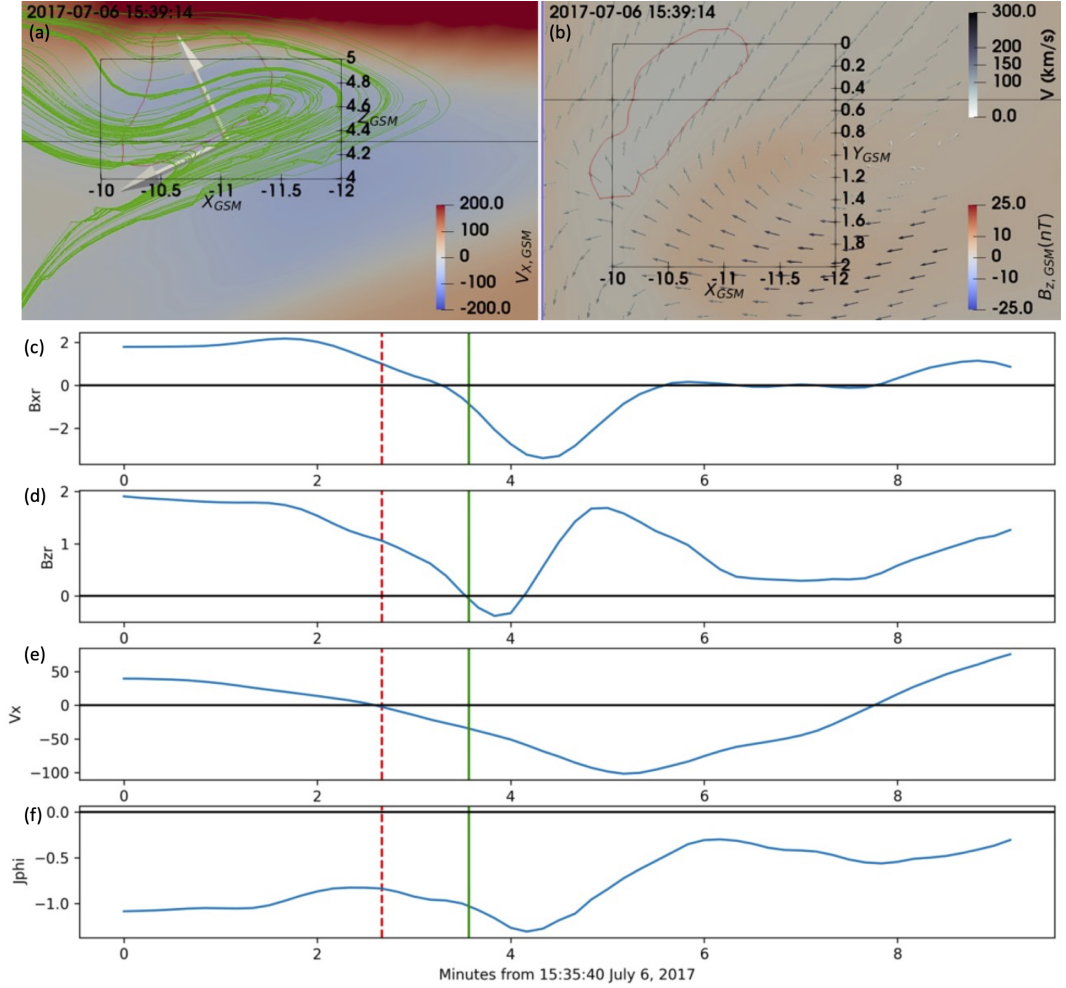


Figure 5. Panels (a) and (b) are similar to Fig. 3 (c) and (d) but zoomed in to show a near Earth x-line at an earlier time. The two tilted axes in panel (a) illustrate the “reconnection” axes for this x-line. Panels (c)–(f) show the reconnecting field ($B_{x,r}$), the reconnected field ($B_{z,r}$), $V_{x,GSM}$, and the azimuthal current in the GSM coordinate system respectively. These quantities are plotted vs time for the position of the x-line as indicated by the origin of the “reconnection” axes ($[x, y, z] = [-11.05, 0.5, 4.31]$). The horizontal black line shows 0 for each quantity, the vertical red dashed line marks the switch from Earthward to tailward flow, and the vertical green line marks when reconnection is observed.

273

6 Conclusion

274 In this paper we have demonstrated the ability to induce reconnection in a global
 275 simulation of Earth's magnetosphere. We did not address the physics of why and how
 276 reconnection was initiated at a particular location but rather imposed localized resistiv-
 277 ity as a means to initiate it in agreement with in situ observations of MMS. This is an
 278 important first step towards incorporating real observations into simulations to create
 279 a more accurate depiction of substorms. With the DM results we can determine places
 280 where x-lines actually form during a substorm and place time dependent patches of lo-
 281 cal resistivity to induce reconnection at correct locations in a global simulation. This is
 282 important since global simulations, and in particular MHD simulations, are missing key
 283 kinetic physics which play an important role in determining the specifics of reconne-
 284 ction. However, the recent results demonstrating the accuracy of DM based reconstruc-
 285 tions of the magnetosphere allow us to implicitly incorporate otherwise missing physics
 286 and correctly simulate the location of reconnection for a given substorm. Future work
 287 will include the time dependent motion of x-lines into our global simulation model.

288 Without any explicit resistivity, an extended x-line often forms far too close to Earth
 289 than we would expect (El-Alaoui et al., 2009; Gong et al., 2021; Bard & Dorelli, 2021;
 290 Park, 2021; Runov et al., 2021). This is a common problem in global simulations of the
 291 magnetosphere. Interestingly, by placing resistivity farther in the tail and inducing re-
 292 connection there, we implicitly suppress reconnection near Earth. This can be explained
 293 simply by noting that reconnection farther in the tail will dipolarize the near Earth mag-
 294 netic field by transporting magnetic flux towards Earth and thus broaden the current
 295 sheet and prevent reconnection. There are no extended x-lines in the near Earth region
 296 for Run Mid, which is consistent with observations of most substorms.

297 A crucial caveat to this conclusion is that we expect smaller scale and shorter lived
 298 x-lines to appear in regions with a tailward flow. As the reconnection exhaust from the
 299 primary x-line in the midtail region reaches the stronger magnetic field near Earth and
 300 rebounds tailward, the magnetic field is stretched due to the frozen in condition. This
 301 stretching of the magnetic field is highly localized in the dawn-dusk direction, limited
 302 to $\sim 5R_E$ at most, and it can create x-lines that last on the order of ~ 10 minutes. Thin
 303 current sheets have been observed as part of the rebounding process (Panov et al., 2010;
 304 Nakamura et al., 2021) and they could lead to reconnection in a similar manner. How-
 305 ever, to the authors' knowledge, these x-lines have not been directly observed. Due to
 306 their small nature both in time and space it would be rare for a satellite to obtain in situ
 307 measurements showing these x-lines. If these x-lines do form near Earth, they could play
 308 an important role in the production of energetic particles. As argued by Angelopoulos
 309 et al. (2020), the average energy per particle is much higher closer to Earth than it is
 310 where typical x-lines form due to the X_{GSM} dependence of the magnetic field strength.
 311 Thus even small scale x-lines could potentially create very energetic particles. This topic
 312 will also need to be explored with test particles in a future paper

313 Note that both near-mid tail X-lines (Run DM_Reconst) and midtail X-lines (Run
 314 Mid) are observed in the DM analysis of substorms (Stephens et al., 2022). In our fu-
 315 ture simulations we plan to use the DM output with 5-min cadence to incorporate the
 316 whole empirical story of X-lines into Gamera simulations. Further efforts will be nec-
 317 essary to also reproduce the multiscale non-MHD structure of the tail current sheet prior
 318 to reconnection onsets.

319

Appendix A Average flows in near Earth secondary x-lines

320 Fig. A1 shows the maximum (red), average (black), and minimum (blue) velocity
 321 in the X_{GSM} direction for each group of x-lines identified in Run Mid that is closer than
 322 $20R_E$ in the tail to Earth. Note, that the average velocity of plasma flows near all these

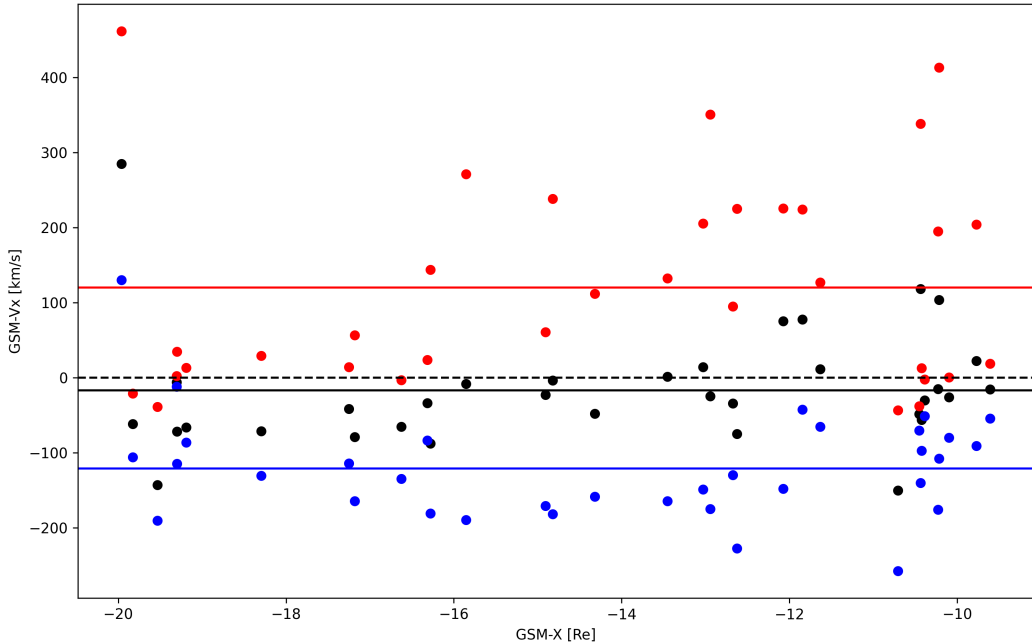


Figure A1. This shows the $V_{X,GSM}$ flow vs X_{GSM} position for all groups of x-lines identified within $20R_E$ of Earth in Run Mid. For each group we plot the maximum Earthward velocity (red), the mean velocity (black), and the minimum velocity (blue). The solid horizontal lines are the average of the maximum (red), mean (black), and minimum (blue) flows. The horizontal black and dashed line marks the difference between Earthward and tailward flows.

x-lines is $\sim -17 \text{ km/s}$. It is important to keep in mind that if the x-lines form in rebounding flows they will be close to the Earthward flow as can be seen in Fig. 3 (d). Since the x-line identification method inherently overestimates the area the x-line occupies we can naturally expect some of the identified “x-lines” to be in the Earthward flow. This explains why the maximum velocity is often Earthward if the x-line forms in tailward flows. However, the average velocity is typically negative further confirming that the x-lines do form in tailward flows.

Appendix B Open Research

The data used in the study are archived on Zenodo (<http://doi.org/10.5281/zenodo.7057795>).

Acknowledgments

This work was funded by NASA grants 80NSSC20K1271 and 80NSSC20K1787, as well as the NSF grant AGS-1744269. This work is supported by the NASA DRIVE Science Center for Geospace Storms (CGS) under Cooperative Agreement 80NSSC22M0163. Joachim Birn acknowledges support by NASA grant 80NSSC18K0834. We thank the reviewers for their assistance in evaluating this paper

References

Angelopoulos, V., Artemyev, A., Phan, T. D., & Miyashita, Y. (2020). Near-earth magnetotail reconnection powers space storms. *Nature Physics*, 16, 317-321.
 Angelopoulos, V., McFadden, J. P., Larson, D., Carlson, C. W., Mende, S. B., Frey,

342 H., ... Kepko, L. (2008). Tail reconnection triggering substorm onset. *Science*,
 343 321(5891).

344 Artemyev, A., Lu, S., El-Alaoui, M., Lin, Y., Angelopoulos, V., Zhang, X.-J., ...
 345 Russell, C. (2021). Configuration of the earth's magnetotail current sheet.
 346 *Geophysical Research Letters*, 48.

347 Baker, D., & P. (1996). Neutral line model of substorms: Past results and present
 348 view. *J. Geophys. Res.: Space Physics*, 101, 12975-13010.

349 Bard, C., & Dorelli, J. (2021). Magnetotail reconnection asymmetries in an ion-
 350 scale, earth-like magnetosphere. *Annales Geophysicae*, 39, 991-1003.

351 Bessho, N., & Bhattacharjee, A. (2014). Instability of the current sheet in the
 352 earth's magnetotail with normal magnetic field. *Physics of Plasmas*, 21.

353 Birn, J., & Hesse, M. (2013). The substorm current wedge in mhd simulations. *Journal*
 354 *of Geophysical Research: Space Physics*, 118, 3364-3376.

355 Birn, J., Hesse, M., & Schindler, K. (1996). Mhd simulations of magnetotail dynam-
 356 ics. *J. Geophys. Res.*, 101, 12939-12954.

357 Birn, J., & Schindler, K. (2002). Thin current sheets in the magnetotail and the loss
 358 of equilibrium. *J. Geophys. Res.*, 107.

359 Coppi, B., Laval, G., & Pellat, R. (1966). Dynamics of the geomagnetic tail. *Physi-
 360 cal Review Letters*, 16.

361 El-Alaoui, M., Ashour-Abdalla, M., Walker, R., Peroomian, V., Richard, R., An-
 362 gelopoulos, V., & Runov, A. (2009). Substorm evolution as revealed by themis
 363 satellites and a globalmhd simulation. *Journal of Geophysical Research*, 114.

364 Gong, F., Yu, Y., & Cao, J. (2021). Simulating the responses of the magneto-
 365 sphere-ionosphere system to the imf by reversal. *Front. Phys.*, 10.

366 Hesse, M., & Birn, J. (1994). Mhd modeling of magnetotail instability for localized
 367 resistivity. *Journal of Geophysical Research*, 99(A5), 8565-8576.

368 Hesse, M., & Schindler, K. (2001). The onset of magnetic reconnection in the mag-
 369 netotail. *Earth, Planets and Space*, 53, 645-653.

370 Imber, S. M., Slavin, J. A., Auster, H. U., & Angelopoulos, V. (2011). A themis sur-
 371 vey of flux ropes and traveling compression regions: Location of the near-earth
 372 reconnection site during solar minimum. *Journal Of Geophysical Research: Space Physics*,
 373 116.

374 Liu, Y.-H., Birn, J., Daughton, W., Hesse, M., & Schindler, K. (2014). Onset of
 375 reconnection in the near magnetotail: Pic simulations. *Journal of Geophysical
 376 Research: Spacec Physics*, 119, 9773-9789.

377 Merkin, V. G., & Lyon, J. G. (2010). Effects of the low-latitude ionospheric bound-
 378 ary condition on the global magnetosphere. *Journal of Geophysical Research:
 379 Space Physics*, 115.

380 Merkin, V. G., Panov, E. V., Sorathia, K. A., & Ukhorskiy, A. Y. (2019). Contribu-
 381 tion of bursty bulk flows to the global dipolarization of the magnetotail during
 382 an isolated substorm. *Journal of Geophyscial Research: Space Physics*, 124.

383 Min, K., Okuda, H., & Sato, T. (1985). Numerical studies on magnetotail formation
 384 and driven reconnection. *Journal of Geophysical Research: Space Physics*, 90,
 385 4035-4045.

386 Nagai, T., Fujimoto, M., Saito, Y., Machida, S., Terasawa, T., Nakamura, R., ...
 387 Kokubun, S. (1998). Structure and dynamics of magnetic reconnection for
 388 substorm onsets with geotail observations. *Journal of Geophysical Research:
 389 Space Physics*, 103, 4419-4440.

390 Nakamura, R., Baumjohann, W., Nakamura, T. K. M., Panov, E. V., Schmid, D.,
 391 Varsani, A., & Apatenkov, S. e. a. (2021). Thin current sheet behind the
 392 dipolarization front. *J. Geophys. Res.*, 126.

393 Nakamura, R., Baumjohann, W., Runov, A., Volwerk, M., Zhang, T. L., Klecker, B.,
 394 ... Frey, H. U. (2002). Fast flow during current sheet thinning. *Geophysical
 395 Research Letters*, 29.

396 Ohtani, S., Miyashita, Y., Singer, H., & Mukai, T. (2009). Tailward flows with posi-
 397 tive bz in the near-earth plasma sheet. *Journal of Geophysical Research*, 114.

398 Panov, E. V., Nakamura, R., Baumjohann, W., Sergeev, V. A., Petrukovich, A. A.,
 399 Angelopoulos, V., ... Larson, D. (2010). Plasma sheet thickness during a
 400 bursty bulk flow reversal. *J. Geophys. Res.*, 115.

401 Park, K. (2021). Global mhd simulation of the weak southward imf condition for dif-
 402 ferent time resolutions. *Front. Astron. Space Sci.*, 8.

403 Pritchett, P. L. (2015). Structure of exhaust jets produced by magnetic reconnection
 404 localized in the out-of-plane direction. *Journal of Geophysical Research*, 120,
 405 592-608.

406 Raeder, J. (1999). Modeling the magnetosphere for northward interplanetary mag-
 407 netic field: Effects of electrical resistivity. *Journal of Geophysical Research: Space
 408 Physics*, 104.

409 Raeder, J. (2003). Global geospace modeling: Tutorial and review. space plasma
 410 simulation. *Lect. Notes Phys.*, 615, 212-246. (Edited by J. Büchner, C. Dum,
 411 and M. Scholer)

412 Raeder, J., Berchem, J., & Ashour-Abdalla, M. (1996). The importance of small
 413 scale processes in global mhd simulations: Some numerical experiments. *The
 414 Physics of Space Plasmas*, 14, 403. (Edited by T. Chang and J. R. Jasperse)

415 Raeder, J., McPherron, R. L., Frank, L. A., Paterson, W. R., Sigwarth, J. B., Lu,
 416 G., ... Slavin, J. A. (2001). Global simulation of the geospace environment
 417 modeling substorm challenge event. *J. Geophys. Res.*, 106.

418 Rogers, A. J., Farrugia, C. J., & Torbert, R. B. (2019). Numerical algorithm for
 419 detecting ion diffusion regions in the geomagnetic tail with applications to
 420 mms tail season 1 may to 30 september 2017. *Journal of Geophysical Research: Space
 421 Physics*, 124, 6487-6503.

422 Runov, A., Grandin, M., Palmroth, M., Battarbee, M., Ganse, U., Hietala, H., ...
 423 Turner, D. (2021). Ion distribution functions in magnetotail reconnection:
 424 global hybrid-vlasov simulation results. *Ann. Geophys.*, 39, 599-612.

425 Runov, A., Nakamura, R., Baumjohann, W., Zhang, T. L., Volwerk, M., Eichel-
 426 berger, H.-U., & Balogh, A. (2003). Cluster observation of a bifurcated current
 427 sheet. *Geophysical Research Letters*, 30.

428 Runov, A., Sergeev, V. A., Baumjohann, W., Nakamura, R., Apatenkov, S., Asano,
 429 Y., ... Rème, H. (2005). Electric current and magnetic field geometry in
 430 flapping magnetotail current sheets. *Annales Geophysicae*, 23, 1391-1403.

431 Runov, A., Sergeev, V. A., Nakamura, R., Baumjohann, W., Apatenkov, S., Asano,
 432 Y., ... Balogh, A. (2006). Local structure of the magnetotail current sheet:
 433 2001 cluster observations. *Annales Geophysicae*, 24, 247-262.

434 Russell, C. T., & McPherron, R. L. (1973). The magnetotail and substorms. *Space
 435 Sciences Reviews*, 15, 205-266.

436 Schindler, K. (1974). A theory of the substorm mechanism. *Journal of Geophysical
 437 Research: Space Physics*, 79.

438 Scholer, M., & Otto, A. (1991). Magnetotail reconnection: Current diversion and
 439 field-aligned currents. *Geophysical Research Letters*, 18, 733-736.

440 Sergeev, V., Angelopoulos, V., Kubyshkina, M., Donovan, E., Zhou, X.-Z., Runov,
 441 A., ... Nakamura, R. (2011). Substorm growth and expansion onset as ob-
 442 served with ideal ground-spacecraft themis coverage. *Journal of Geophysical
 443 Research: Space Physics*, 116.

444 Sergeev, V., Runov, A., Baumjohann, W., Nakamura, R., Zhang, T. L., Volwerk, M.,
 445 ... Klecker, B. (2003). Current sheet flapping motion and structure observed
 446 by cluster. *Geophysical Research Letters*, 30.

447 Sitnov, M. I., Buzulukova, N., Swisdak, M., Merkin, V. G., & Moore, T. E. (2013).
 448 Spontaneous formation of dipolarization fronts and reconnection onset in the
 449 magnetotail. *Geophysical Research Letters*, 40.

450 Sitnov, M. I., & Schindler, K. (2010). Tearing stability of a multiscale magnetotail
451 current sheet. *Geophysical Research Letters*, 37.

452 Sorathia, K. A., Merkin, V. G., Panov, E. V., Zhang, B., Lyon, J. G., & Garretson,
453 e. a., J. (2020). Ballooning-interchange instability in the near-earth plasma
454 sheet and auroral beads: Global magnetospheric modeling at the limit of the
455 mhd approximation. *Geophys. Res. Lett.*, 47.

456 Stephens, G., Sitnov, M., Korth, H., Tsyganenko, N. A., Ohtani, S., Gkioulidou, M.,
457 & Ukhorskiy, A. Y. (2019). Global empirical picture of magnetospheric sub-
458 storms inferred from multimission magnetometer data. *Journal of Geophysical
459 Research: Space Physics*, 124, 1085-1110.

460 Stephens, G. K., Sitnov, M. I., Weigel, R. S., Turner, D. I., Tsyganenko, N. A.,
461 Rogers, A. J., ... Slavin, J. A. (2022). Global structure of magnetotail recon-
462 nection revealed by mining space magnetometer data. *Earth and Space Science
463 Open Archive*. doi: 10.1002/essoar.10511996.1

464 Torbert, R. B., Burch, J. L., Phan, T. D., Hesse, M., Argall, M. R., Shuster, J., &
465 Ergun, R. E. e. a. (2018). Electron-scale dynamics of the diffusion region
466 during symmetric magnetic reconnection in space. *Science*, 362, 1391-1395.

467 Ugai, M., & Tsuda, T. (1979). Magnetic field-line reconnection by localized enhance-
468 ment of resistivity. part 4. dependence on the magnitude of resistivity. *Journal
469 of Plasma Physics*, 22, 1-14.

470 Zhang, B., Sorathia, K., Lyon, J., Merkin, V., Garretson, J., & Wiltberger, M.
471 (2019). Gamera: A three-dimensional finite-volume mhd solver for non-
472 orthogonal curvilinear geometries. *The Astrophysical Journal*, 244.

473 Zhang, L. Q., Liu, Z. X., Ma, Z. W., Baumjohann, W., Pu, Z. Y., Dunlop, M. W.,
474 ... Wang, J. Y. (2010). X line distribution determined from earthward and
475 tailward convective bursty flows in the central plasma sheet. *Journal of Geo-
476 physical Research*, 115.

477 Zhao, S., Tian, A., Shi, Q., Xizo, C., Fu, S., Zong, Q., ... Tan, K. (2016). Statistical
478 study of magnetotail flux ropes near the lunar orbit. *Science China Technologi-
479 cal Sciences*, 59, 1591-1596.